Polypropylene/Nylon 6 Blends: Phase Distribution Morphology, Rheological Measurements, and Structure Development in Melt Spinning

BO-RUN LIANG,* JAMES L. WHITE, JOSEPH E. SPRUIELL, and BHUVENESH C. GOSWAMI,† *Polymer Engineering, University of Tennessee, Knoxville, Tennessee 37996*

Synopsis

A series of polypropylene (PP)/nylon 6 (N6) blends of composition 75/25, 50/50, and 25/75 have been prepared in a screw extruder combined with a Koch static mixer. The phase morphology was observed with a scanning electron microscope. The influence of heating in the reservoir of a rheometer followed by subsequent extrusion through a capillary on the phase morphology was investigated. Phase size growth as a function of time was observed under quiescent and mild deformation rate conditions. The discrete phase size was observed to decrease with increasing extrusion rate through dies. The shear viscosity and principal normal stress difference of the blends were measured as a function of composition. The crystalline orientation of both polypropylene and nylon 6 in blend melt spun fibers was characterized by wide angle X-ray diffraction and interpreted in terms of Hermans–Stein orientation factors. The orientation increases with drawdown ratio. The orientation factors for the polypropylene phase vary with spinline stress in a manner independent of composition and identical to that for pure polypropylene. Extracting melt spun blend fibers with formic acid has produced small-diameter polypropylene minifilaments with diameters of the order of microns.

INTRODUCTION

There have been extensive investigations through the years of characteristics of blends of thermoplastics. Most of these studies have involved polyolefins and styrenics. Few have involved polyamides. Some reports have appeared of blends of polyamides with polyethylene terephthalate,[1-3] polyethylene,[4] polypropylene,[5,6] polyoxymethylene,[7-10] butadiene–acrylonitrile copolymer,[11] and other polyamides.[12] These studies have usually involved nylon 6.[1-6,11,12] None of these papers contains a vertically integrated investigation of the melt rheology, phase morphology, and processing of such blends.

In the present paper, we consider various aspects of the disperse two-phase melt flow and solidification of polypropylene/nylon 6 blends including the structure of the products produced. We will investigate the (i) phase morphology and how it varies with process conditions, (ii) the rheological properties of the blends, (iii) the development of structure during the melt spinning of fibers, and (iv) the formation of small-diameter minifibers by extracting blend filaments. This paper represents one of the broadest vertically integrated studies of a polymer blend system.

* Permanent address: Department of Textile Chemistry, East China Institute of Textile Science and Technology, Shanghai, People's Republic of China.

† Department of Textiles, Merchandising and Design.

Journal of Applied Polymer Science, Vol. 28, 2011–2032 (1983)

CCC 0021-8995/83/062011-22$03.20

EXPERIMENTAL

Materials

The polymers used in this study were an isotactic polypropylene (PP) (Hercules Profax PD 064 with melt index of 3.5) and nylon 6 (N6) supplied by American Enka. The latter material had a M_n = 22,500 and M_w/M_n = 2.08.

Blending

The polypropylene (PP) and nylon 6 (N6) were mixed in a ¾ in. Rainville screw extruder with a Koch static mixer at 230°C. Blends with composition PP/N6 of 75/25, 50/50, and 25/75 were prepared.

Scanning Electron Microscopy (SEM)

The SEM studies were carried out using an AMR Model 900 High Resolution Scanning Electron Microscope (Advanced Metals Research Corporation, Burlington, Mass.). Fracture surfaces of the extrudates of PP/N6 blends from extruder with a static mixer and from capillary die were prepared. A gold palladium alloy was used on the surfaces to prevent charging in the electron beam.

Rheological Measurements

The melt flow rheological properties of the homopolymers and blends were determined at 230°C in both a Rheometrics Mechanical Spectrometer in the cone-plate mode and in a Merz-Colwell Instron Capillary Rheometer.

Shear stresses σ_{12} and principal normal stress differences $N_1(\sigma_{11}-\sigma_{22})$ were obtained as a function of shear rate in the cone-plate instrument. The shear rate $\dot{\gamma}$ is given by the angular velocity Ω and the cone angle α[13,14]

$$\dot{\gamma} = \Omega/\alpha \tag{1}$$

while the shear stress is given by the torque M and the principal normal stress difference by the thrust F, through[13,14]

$$\sigma_{12} = 3M/2\pi R^3 \tag{2}$$

$$N_1 = 2F/\pi R^2 \tag{3}$$

Measurements were possible up to a shear rate of 1 s^{-1}, where the melts generally balled up and came out of the gap.

At high shear rates the viscosities were determined using a capillary rheometer. The shear stress was measured through the pressure loss through a series of three capillary dies of diameter, D, 0.735 mm and (length)/(diameter) (L/D) 20, 30, 40. The pressure p_T was plotted as a function of die L/D and the die wall shear stress $(\sigma_{12})_w$ was determined from[14,15]

$$p_T = 4(\sigma_{12})_w L/D + \Delta p_{\text{ends}} \tag{4}$$

where Δp_{ends} is the sum of die entrance and exit pressure losses. The die wall shear rate was determined from Weissenberg's relationship[13,14]

$$\dot{\gamma}_w = \frac{3n' + 1}{4n'} \frac{32Q}{\pi D^3} \tag{5}$$

where

$$n' = \frac{d \log(\sigma_{12})_w}{d \log 32Q/\pi D^3} \tag{6}$$

Melt Spinning

Fibers were melt spun through a single hole spinneret capillary with diameter 0.735 mm and L/D ratio of 40 placed in an Instron capillary rheometer. The extrusion temperature was 230°C. The filament descended from the die into a water quench bath, around a roller and onto a takeup device with a takeup speed 17–55 m/min depending on drawdown ratio. Spinline tensions were measured with a Rothschild Tensiometer. The experimental procedure is basically that used by Minoshima et al.[16] in an earlier study in our laboratories.

Characterization of Fiber Structure

The orientation of the crystalline regions of both the polypropylene and nylon 6 phases were measured by wide-angle X-ray diffraction. Nickel-filtered CuKα radiation was used.

Both the polypropylene and nylon 6 diffract X-rays. Typical equatorial intensity scans as a function of Bragg angle for monoclinic polypropylene and the pseudohexagonal nylon 6 found in a melt spun fiber are shown in Figure 1. The WAXS reflections of monoclinic polypropylene in terms of its unit cell have been

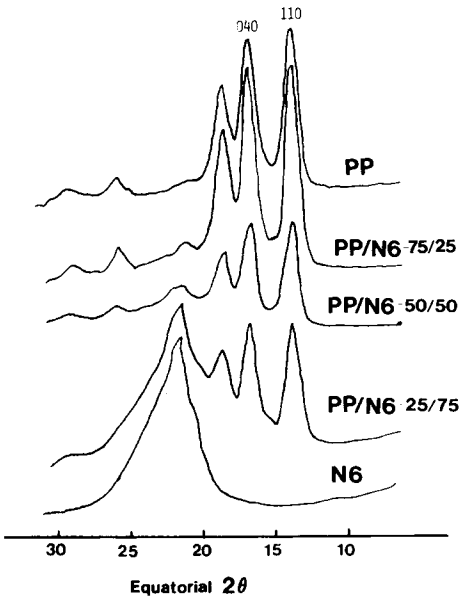

Fig. 1. 2θ scan for monoclinic polypropylene and pseudohexagonal nylon 6.

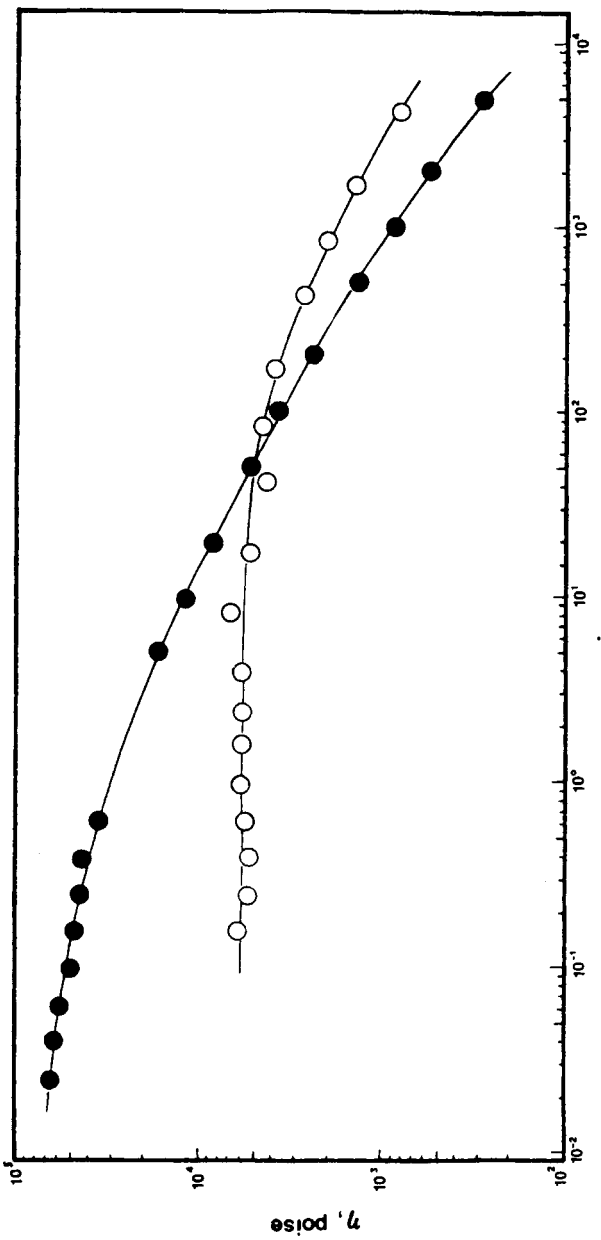

(a)

Fig 2. (a) Viscosity η as a function of shear rate for polypropylene (●) and nylon 6 (○), T = 230°C; (b) Principal normal stress difference as a function of shear rate for polypropylene (●) and nylon 6 (○).

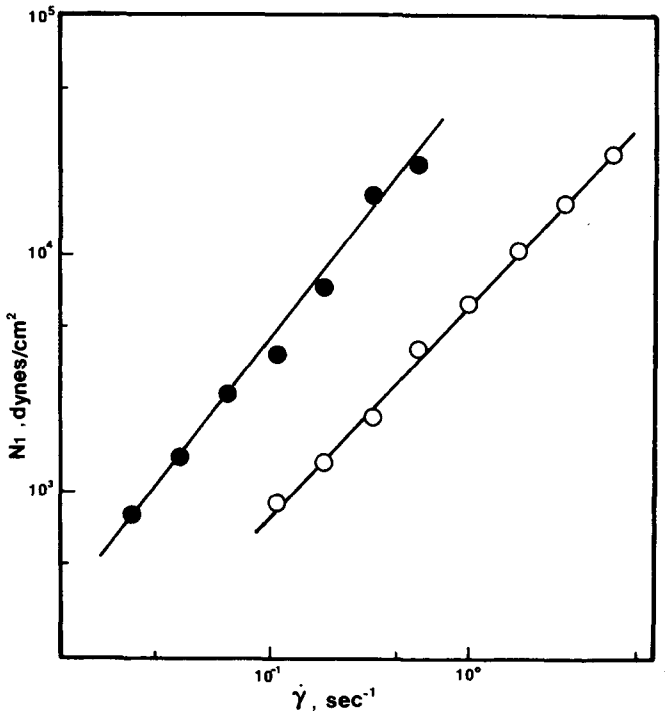

(b)

Fig. 2. (*Continued from the previous page.*)

described by Natta and Corradini.[17] The reflections for nylon 6 are described by Ziabicki,[18] Vogelsong,[19] and Parker and Lindenmeyer.[20]

There is some overlap of peaks. However, the 040 and 110 diffraction peaks of polypropylene are not so encumbered. The 040 and 110 reflections may be used to specify orientations of the crystallographic axes. Pseudohexagonal nylon 6 does not exhibit the range of reflections that monoclinic polypropylene does. Usually the 100 and 002 reflections are used to determine the orientation of the crystallographic axes. It is not possible to use the 100 reflection here because of peak overlap.

We shall represent orientation in terms of the Hermans–Stein orientation factors for the three crystallographic axes.[21-23] These are defined as

$$f_j = (3\,\overline{\cos^2\phi_j} - 1)/2 \tag{7}$$

where ϕ_j is angle between the fiber axis and the j-crystallographic axis. The 040 reflection directly gives the orientation of the b-crystallographic axis. The orientation of the c-crystallographic axis can be obtained from the 110 and 040 reflections through Wilchinsky's expression[24]

$$\cos^2\phi_c = 1 - 1.099\cos^2\phi_{110,1} - 0.901\cos^2\phi_{040,1} \tag{8}$$

For the orientation of the pseudohexagonal nylon 6 in the melt-spun fibers we used the meridional 002 reflection. An a'-crystallographic axis was defined to

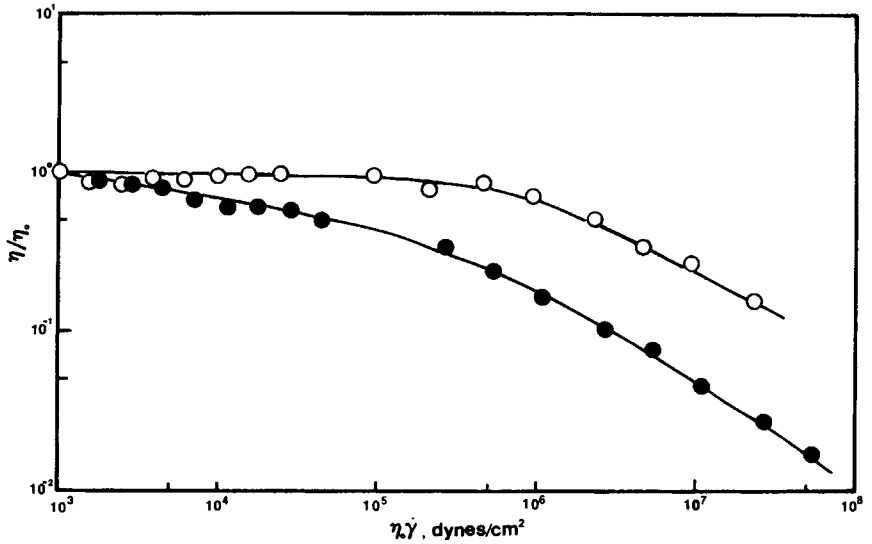

Fig. 3. Reduced viscosity η/η_0 as a function of $\eta_0\dot{\gamma}$ for polypropylene (●) and nylon 6 (○).

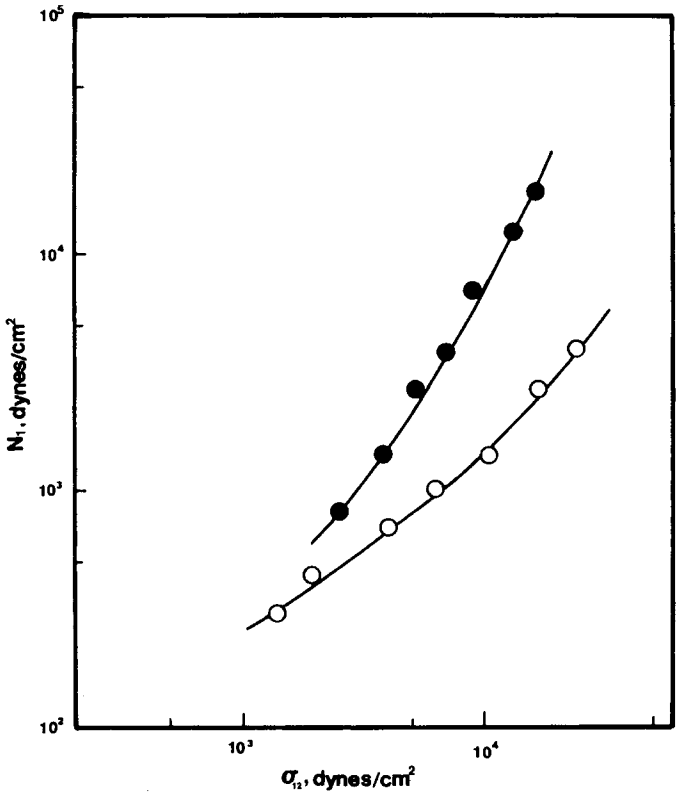

Fig. 4. Principal normal stress difference N_1, as a function of shear stress σ_{12}, for polypropylene (●) and nylon 6 (○).

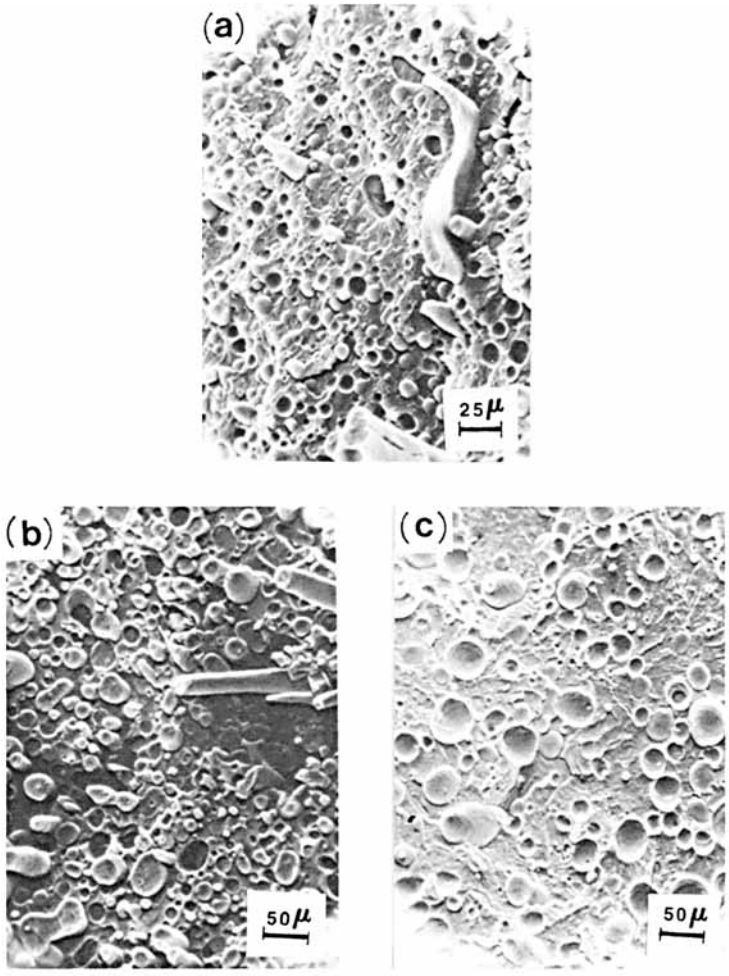

Fig. 5. SEM photomicrographs of PP/N6 blends prepared in a screw extruder and Koch static mixer: (a) 75/25; (b) 50/50; (c) 25/75.

be perpendicular to the plane of the b and c axes. We will define from this an orientation factor $f_{a'}$ (compare Nadella et al.[22]).

Extraction of Filaments

The melt-spun PP/N6 75/25, 50/50, and 25/75 filaments were extracted in formic acid. This would remove the nylon 6 and leave the polypropylene. The character of the extracted filaments were investigated using scanning electron microscopy.

RHEOLOGICAL PROPERTIES OF PURE COMPONENTS

The shear viscosity η and principal normal stress difference N_1 were measured for both the polypropylene and nylon 6 at 230°C in the Rheometrics Mechanical

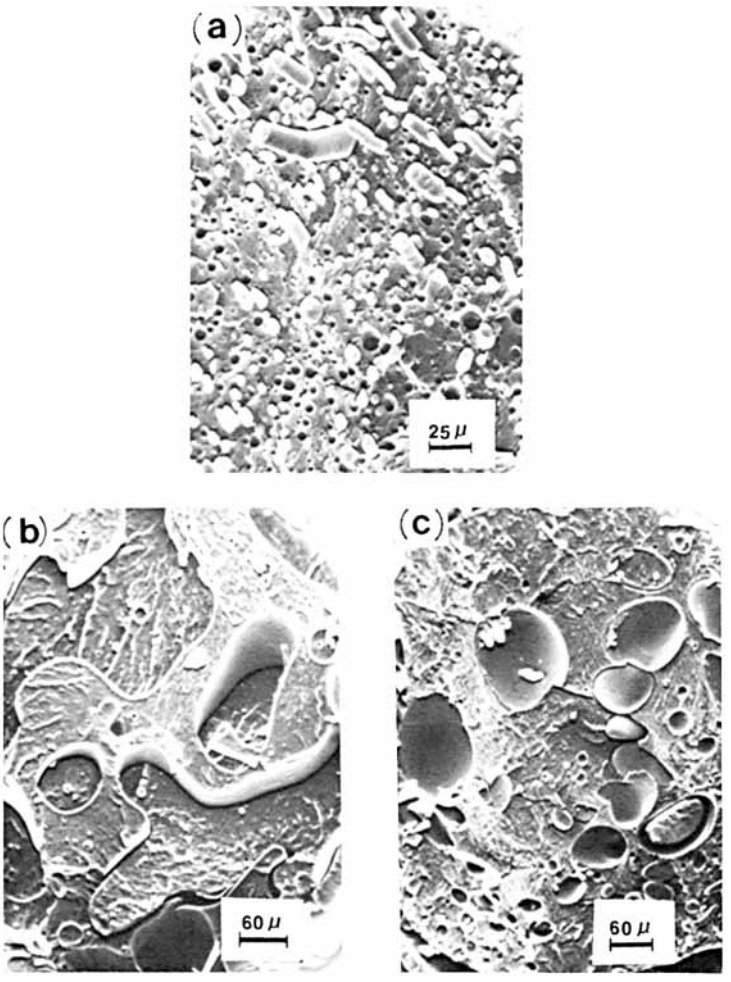

Fig. 6. SEM photomicrographs of PP/N6 blend extrudates heated for a period of 60 min and extruded at $32Q/\pi D^3$ of 3.79 s^{-1} through a capillary die: (a) 75/25; (b) 50/50; (c) 25/75.

Spectrometer. Viscosities of higher shear rates were measured in the capillary rheometer. The results are shown in Figure 2. At low shear rates, the PP exhibits both a higher viscosity and a higher principal normal stress difference than nylon 6. The zero shear rate viscosity η_0 for PP is of order 80,000 P and for nylon 6 of order 6,000 P. The nylon 6 viscosity function is much more Newtonian in character than the PP, and there is a crossover at about 60 s^{-1}.

The differences in the rheological properties of the nylon 6 and PP seem due to a combination of absolute molecular weight and breadth of molecular weight distribution, as suggested by recent studies from our laboratory.[25–27] The differences in zero shear viscosity indicated that the PP has a much higher molecular weight. In Figures 3 and 4, we plot η/η_0 vs. $\eta_0\dot{\gamma}$ and N_1 vs. σ_{12} for the two melts. The PP data fall off more rapidly than the nylon 6 in the η/η_0 vs. $\eta_0\dot{\gamma}$ plot and are higher than the nylon 6 data in the N_1–σ_{12} plot. Both indicate the broader molecular weight distribution of PP.[25–27]

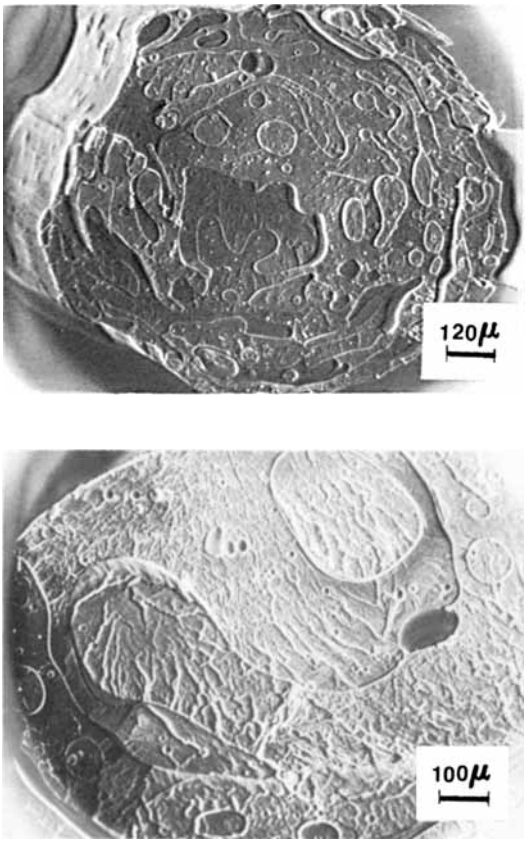

Fig. 7. SEM photomicrographs of 50/50 PP/N6 blends removed from reservoir after being heated for various periods: (a) 30 min; (b) 180 min.

PHASE MORPHOLOGY

Extrudates from Screw Extruder/Static Mixer System

Extrudates from the static mixer were cross-sectioned. SEM photomicrographs are shown in Figure 5. The PP/N6 25/75 blends show polypropylene islands in a nylon 6 sea. Both 75/25 and 50/50 blends show nylon 6 islands in a polypropylene sea. The cross sections of the discrete islands have dimensions of 5–50 μm depending on composition. The smaller dimensions are found in the PP/N6 75/25 blends and the coarser morphology in the 50/50 and 25/75 blends.

Blend Melt in a Heated Reservoir and Subsequent Extrusion from Capillary Die

The extrudates from the static mixer were placed in the barrel of the Instron capillary rheometer and heated at 230°C. After various periods, the melt was extruded at a low rate, equivalent to a die wall shear rate of 3.79 s^{-1} and shear

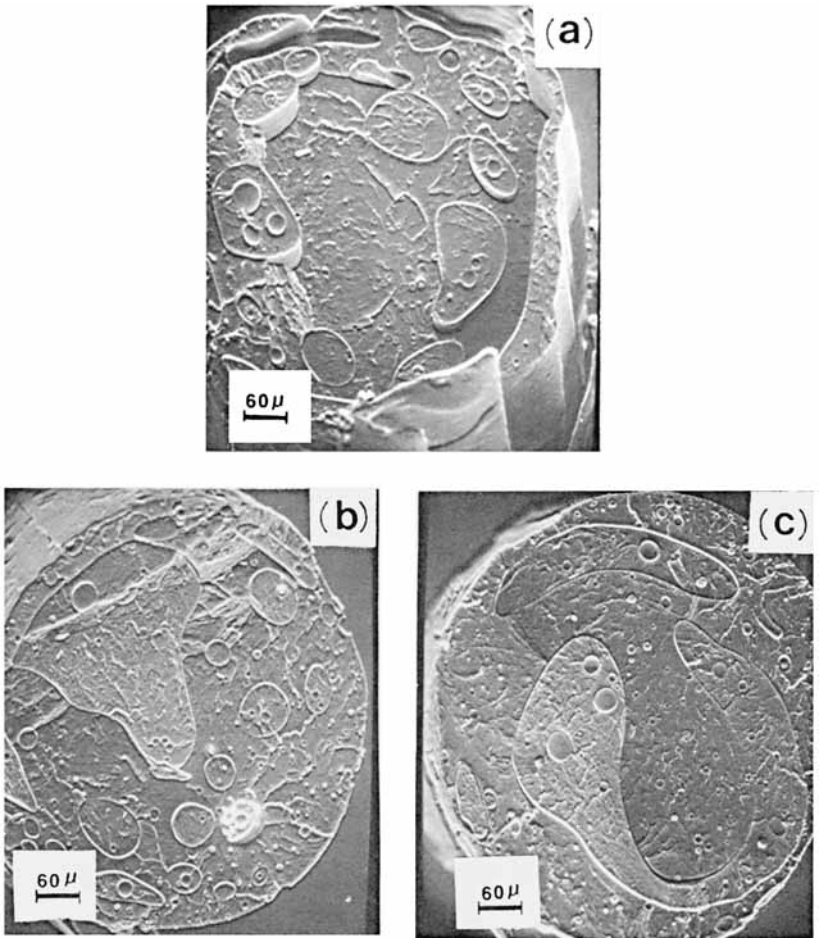

Fig. 8. SEM photomicrographs of PP/N6 50/50 blends extruded from a capillary die at $32Q/\pi D^3$ of 3.79 s^{-1}, T = 230°C for (a) 30 min, (b) 90 min, (c) 150 min.

stress of order 0.5×10^5 dyn/cm^2. SEM photomicrographs of the extrudates are shown in Figure 6. It may be seen that in the 25/75 and 50/50 PP/N6 blends, the islands grow in size with time. Phase dimensions of order 60–100 μm are observed after 1 h. Little change is observed in the 75/25 blends. In Figures 7 and 8 we observe phase morphologies of the 50/50 blend extrudates from barrel and capillary die with different residence times. A similar phenomenon was observed. The increase in phase dimensions with time is clear.

We have studied the influence of extrusion rate on the morphology of the PP/N6 blends. This is shown in Figures 9–11. As the extrusion rate increases, the sizes of the phase dimensions become smaller (see Table I). We plot island size vs. die wall shear stress $(\sigma_{12})_w$ in Figure 12 for the 75/25 and 25/75 blends.

Discussion

Both Ide and Hasegawa[5] and Baramboim and Rakityanskii[6] have noted that

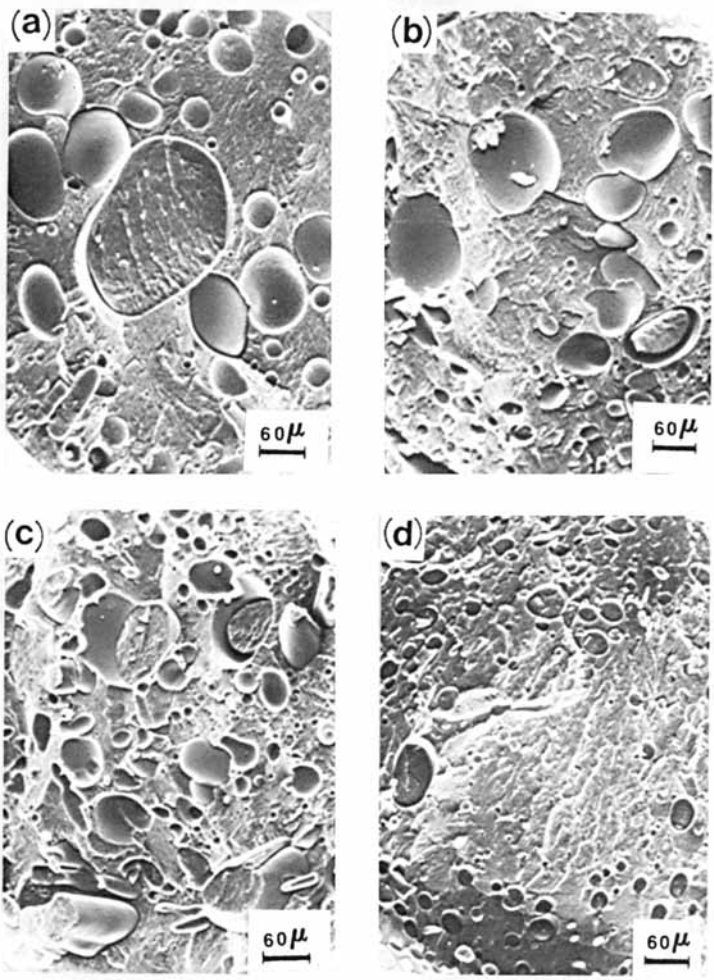

Fig. 9. SEM photomicrographs of PP/N6 25/75 blend extrudates as a function of die wall shear rate $32Q/\pi D^3$: (a) 3.79 s^{-1}; (b) 37.9 s^{-1}; (c) 152 s^{-1}; (d) 1520 s^{-1}.

PP/N6 blends are difficult to disperse in comparison to blends of polymers of similar character. However, the growth in coarseness of the morphology in the molten state for this blend system has not been previously observed. Observations in our laboratories for similarly prepared polyethylene–polystyrene blends[28] show much more fine-grained morphologies (1–5 μm) and no noticeable phase growth with time. The phenomenon thus apparently does not occur in purely hydrocarbon melts.

Ide and Hasegawa[5] and Baramboim and Rakityanskii[6] note that addition of small amounts of additives such as maleic anhydride-grafted polypropylene could produce much finer dispersions. The latter authors attribute this to reductions in interfacial tension.

It appears to us that the mechanism of transient phase growth particularly of PP islands in an N6 sea is associated with the interfacial tension K between the phases. This should lead to stresses of form K/d, where d represents a radius

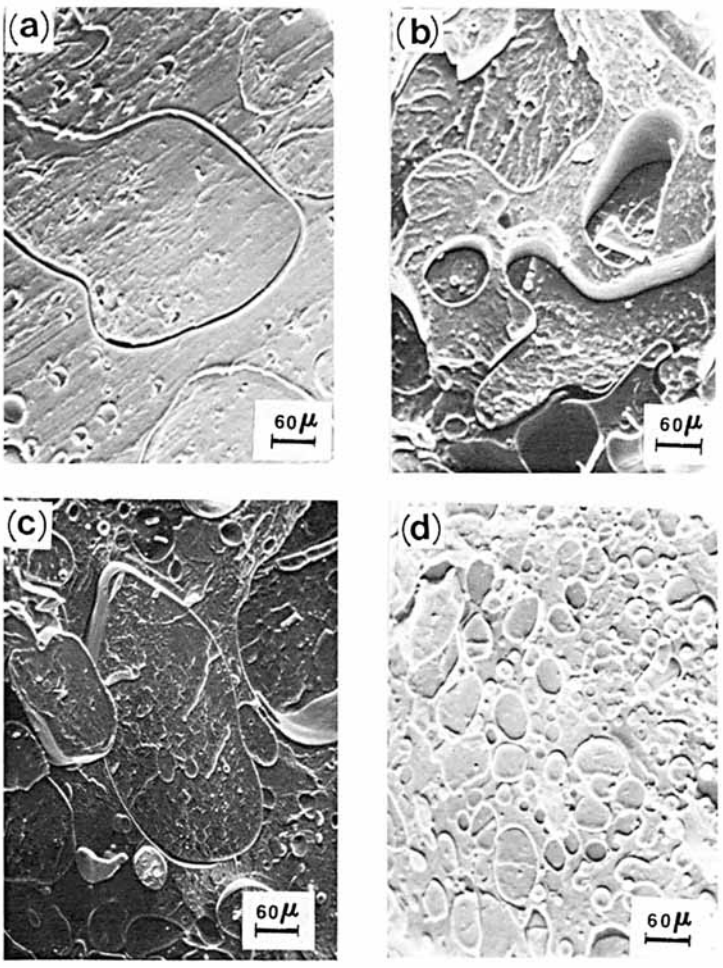

Fig. 10. SEM photomicrographs of 50/50 extrudates as a function of die wall shear rate $32Q/\pi D^3$: (a) 3.79 s^{-1}; (b) 37.9 s^{-1}; (c) 379 s^{-1}; (d) 3790 s^{-1}.

of curvature which will be of the same order as the dimensions of the PP island. The resistance to interfacial movement will be due to the viscosity η of the continuous phase. This is of form $\eta V/d$, where V is a velocity. The tendency of different blend systems towards phase growth is determined by the ratio of these stresses

$$\frac{\text{interfacial stresses}}{\text{viscous stresses}} = \frac{K/d}{\eta V/d} = \frac{K}{\eta V} \tag{9}$$

This dimensionless group is well known in the theory of emulsions of Newtonian fluids.[29–31] It is useful to write eq. (9) in the form

$$\frac{K}{\eta V} \simeq \frac{K}{\eta \dot{\gamma} d} \simeq \frac{K}{\sigma d} \tag{10}$$

Phase growth is promoted by large interfacial tensions, small shear stresses, and small phase dimensions. Phase size reduction is promoted by large shear stresses

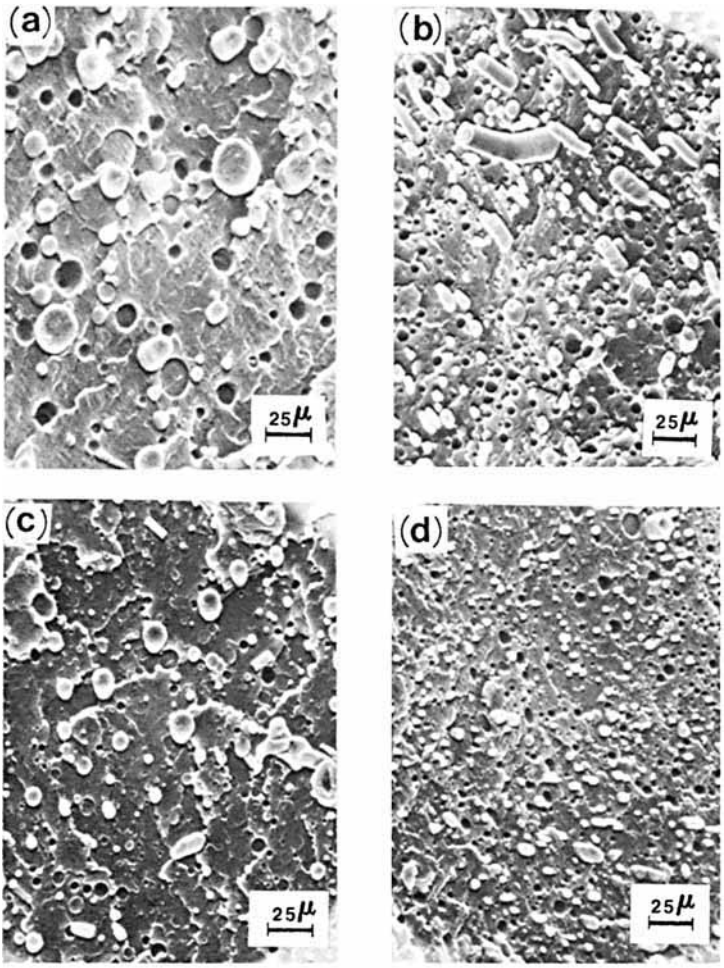

Fig. 11. SEM photomicrographs of PP/N6 75/25 extrudates as a function of die wall shear rate $32Q/\pi D^3$: (a) 3.79 s^{-1}; (b) 37.9 s^{-1}; (c) 152 s^{-1}; (d) 1520 s^{-1}.

and phase dimensions and is opposed by the interfacial tension.

RHEOLOGICAL PROPERTIES OF BLENDS

Results

The viscosity–shear rate behavior of nylon 6, PP and their blends are shown in Figure 13. The viscosity of the blends is plotted as a function of composition at fixed shear rate in Figure 14. As shown in Figures 13 and 14, the viscosity varies with composition in a complicated manner. It exhibits a minimum and maximum in the plot.

A principal normal stress difference N_1–shear rate $\dot{\gamma}$ plot for the blends is shown in Figure 15. The value of N_1 is a monotonic increasing function of both shear rate and PP content over most of the composition range. The data is replotted as a function of shear stress in Figure 16. This indicates that the 75/25 and 50/50 blends exhibit higher N_1 at fixed σ_{12} than either pure component.

TABLE I
The Influence of Extrusion Conditions on the Dimensions of the Discrete Islands of PP/N6 Blends

Composition	$\dot{\gamma}_w$ (s-1)	$(\sigma_{12})_w \times 10^{-5}$ (dyn/cm^2)	Average size of discrete phase (μm)
PP/N6-25/75	3.79	0.31	29
	37.9	1.61	25
	152	4.01	23.5
	3790	20.3	14.5
PP/N6-75/25	3.79	0.36	7.7
	37.9	1.91	4.8
	152	2.65	3.8
	1520	9.20	2.2

Discussion

There are few other investigations of nylon 6–polyolefin blends in the literature. Hayashida et al.[4] found a monotonic increase in viscosity with addition of polyethylene to nylon 6. They sought to represent the viscosity–composition behavior of the blends using a model developed by Lees.[32] This presumes a parallel lamellar structure in the direction of flow with a constant shear stress within the layers. This leads to the expression

$$\frac{1}{\eta} = \frac{\phi}{\eta_{N6}} + \frac{1-\phi}{\eta_{PP}} \tag{11}$$

where ϕ is the volume fraction of nylon 6. We contrast this to experiment in Figure 17 where we plot shear viscosity as a function of composition at different

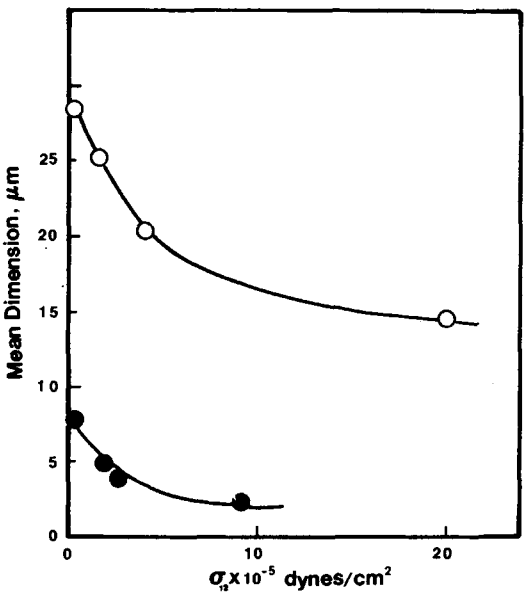

Fig. 12. Mean dimensions of islands in 75/25 (●) and 25/75 (○) PP/N6 blends as a function of die wall shear stress.

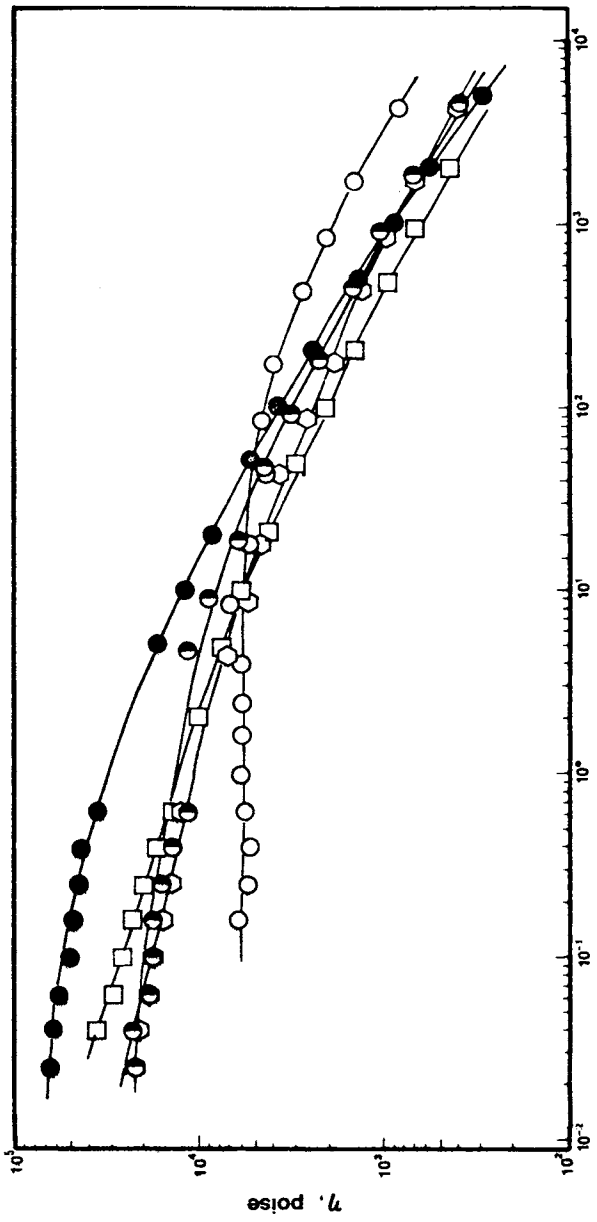

Fig. 13. Viscosity shear rate behavior (T = 230°C) of nylon 6 (○), polypropylene (●), and PP/N6 blends: (□) 75/25; (◑) 50/50; (○) 25/75.

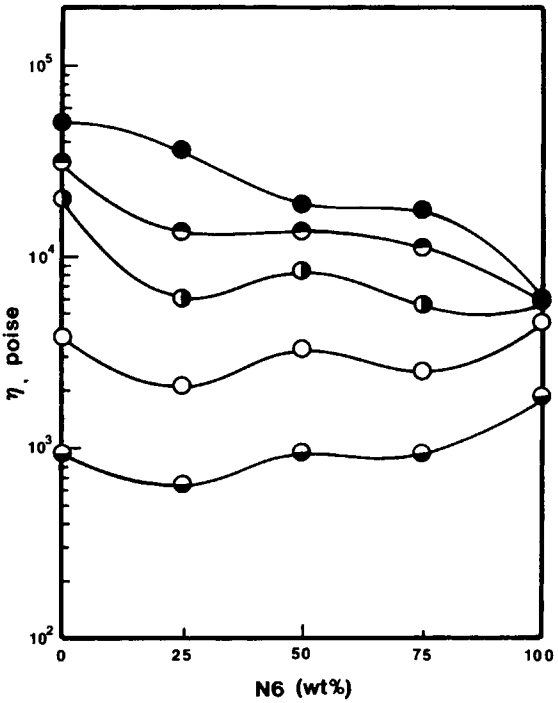

Fig. 14. Viscosity–composition plot for PP/N6 blends at various shear rates $\dot{\gamma}$ (s^{-1}): (●) 10^{-1}; (◓) 10^0; (◑) 10^1; (○) 10^2; (◒) 10^3.

shear stresses. The agreement is not good. Certainly the situation is more complex than envisaged in this model.

STRUCTURE OF MELT-SPUN FIBERS

Results

WAXS patterns for the nylon 6, polypropylene, and PP/N6 blends are shown in Figure 18. The nylon 6 fibers exhibit diffraction patterns similar to those reported by Ziabicki[18] and Bankar et al.[23] with diffuse meridional and equatorial spots. The polypropylene exhibits diffraction patterns equivalent to that described by Natta and Corradini[17] and Nadella et al.[22] These correspond to pseudohexagonal nylon 6 and monoclinic polypropylene. The diffraction pattern of the PP/N6 blends indicate a superposition of pseudohexagonal nylon 6 and monoclinic polypropylene.

With increasing drawdown, the WAXS patterns indicate increased orientation. Hermans–Stein orientation factors f_a', f_b, f_c have been computed for polypropylene and f_c' for nylon 6. The orientation of both phases in the blends was determined. The polypropylene orientation factors are plotted as a function of spinline stress in Figure 19. The results show that the molecular orientation in the polypropylene component of the blends is independent of blend composition when compared on the basis of spinline stress. The 040 reflection becomes equatorial, and f_b becomes negative indicating the b-crystallographic axis is

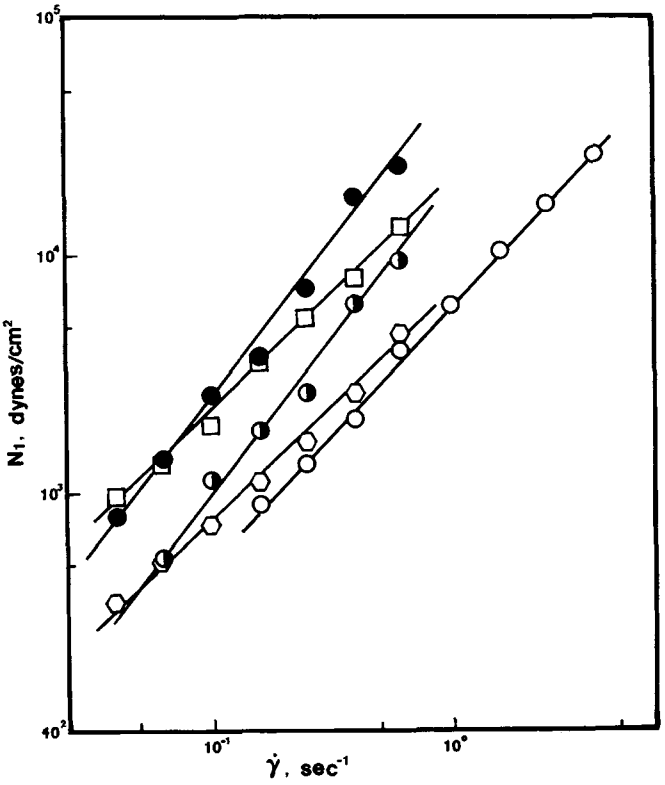

Fig. 15. Principal normal stress difference N_1–shear rate $\dot{\gamma}$ plot for nylon 6 (○), polypropylene (●), and PP/N6 blends: (□) 75/25; (◑) 50/50; (○) 25/75.

perpendicular to the fiber direction. The f_c values computed by Wilchinsky's formula increase monotonically with drawdown stress.

In Figure 20 we plot f_c' for nylon 6 and nylon 6 component in the blends as function of drawdown stress. The data for the 25/75 and 50/50 compositions are much lower than for the pure components.

Discussion

We have contrasted our results for PP and nylon 6 to earlier data in the literature. Spruiell and White,[33] Nadella et al.,[22] and Chen et al.[34] have reported plots of Hermans–Stein orientation factors, f_a', f_b, and f_c as a function of spinline stress for polypropylene. Gianchandani et al.[35] have prepared a similar plot for nylon 6. Our results for pure PP and nylon 6 generally agrees with those of these earlier investigators.

The data for the crystalline orientation factor of nylon 6 in the blends is lower than that for the pure nylon 6. We believe that this in large part is due to overlap of the nylon 6 002 ($2\theta = 11°$) with (i) the much stronger PP 110 ($2\theta = 14.2°$) and (ii) background and amorphous scattering which become relatively stronger as the amount of N6 decreases. A careful inspection of Figure 19 shows a similar effect for PP in the 25/75 PP/N6 blend with the orientation being noticeably,

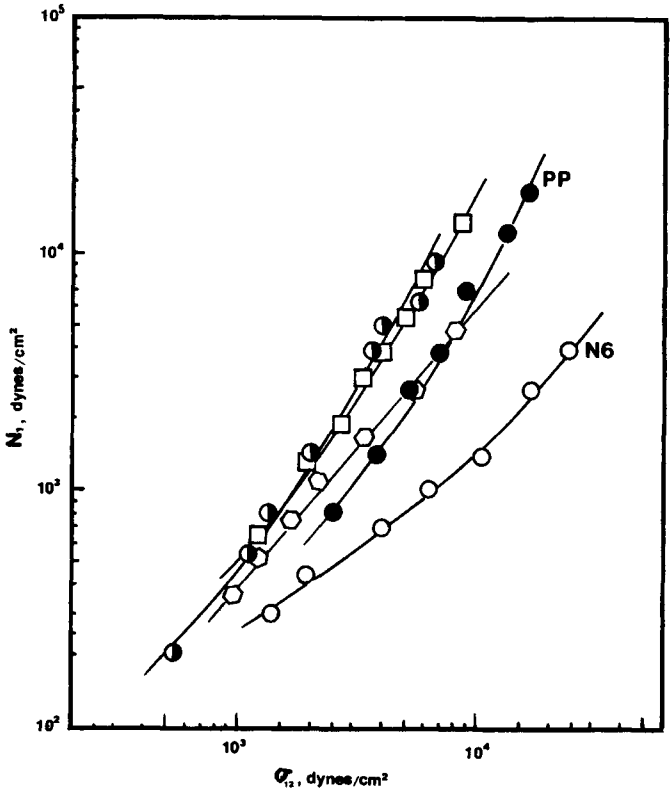

Fig. 16. Principal normal stress difference N_1–shear stress σ_{12} plot (T = 230°C) for nylon 6 (○), polypropylene (●), and PP/N6 blends: (□) 75/25; (◑) 50/50; (○) 25/75.

though only slightly, lower than the data for the other blends. One cannot, of course, say that if such errors were not present the nylon 6 orientation factors in the blends would correlate with stress. It can only be said that with increasing PP, the uncertainty rapidly increases, and ignoring this will lead to lower and lower Hermans orientation factors.

The correlation of the PP orientation in blends with spinline stress is reasonable if one considers the observations of earlier authors on the online spinline structure development for PP and N6 individually. Observations for PP[22,33,36] indicate that it crystallizes in the spinline at a temperature of about 90°C. Nylon 6 vitrifies in the spinline, probably at about 40°C. On the bobbin it absorbs moisture which lowers T_g and then crystallizes. One may consider either a PP continuous phase or a longitudinal cocontinuous phase with PP islands being long minifilaments (see the next section). The spinline tension appropriately corrected to stress will act on the PP phase as it crystallizes. This reasonably leads to a correlation between crystalline orientation and spinline stress in PP, which would be the same as for melt-spun fibers from the pure polymer.

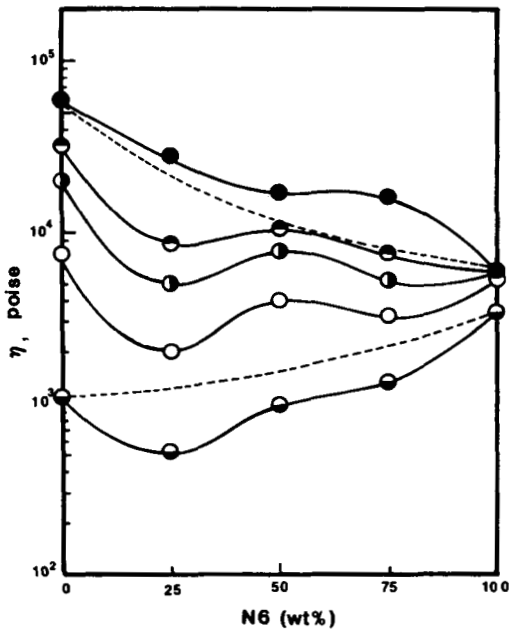

Fig. 17. Viscosity-composition plot at different shear stresses σ_{12} (dyn/cm^2), in comparison with Lee's equation [eq. (11)]: (●) 2×10^3; (◓) 4×10^4; (◑) 10^5; (○) 3×10^5; (◒) 10^6.

EXTRACTION OF MELT-SPUN FILAMENTS

Results

Formic acid-extracted PP/N6 blend melt spun fibers are shown in Figure 21. Small-diameter "mini" filaments that have diameters in a range of 0.5–5 μm are obtained from the 25/75 PP/N6 blends and porous fibers from the 75/25 blend. These minifilaments seem to be potentially infinitely long.

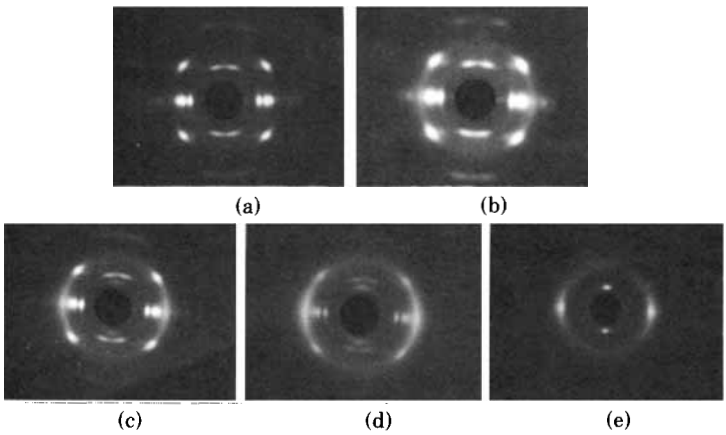

Fig. 18. WAXS film patterns for nylon 6, polypropylene, and N6/PP melt-spun fibers v_L/v_0 = 257: (a) PP; (b) N6/PP 25/75; (c) N6/PP 50/50; (d) N6/PP 25/75; (e) N6.

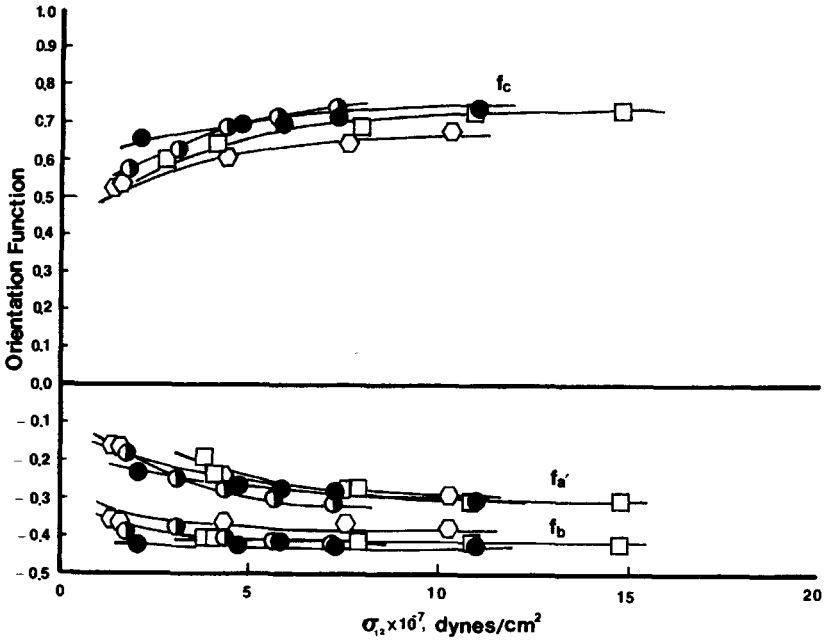

Fig. 19. Hermans–Stein orientation factors f_a', f_b, and f_c as a function of spinline stress, for PP fraction of the blends: (●) PP; (□) PP/N6 75/25; (◑) PP/N6 50/50; (○) PP/N6 25/75.

Discussion

Similarly prepared mini fibers have been reported by investigators in various laboratories[7–10,37–41] using a number of different polymer systems though not nylon 6/polypropylene. Some of these systems have included polyamides[7–10,38,41] and polypropylene[41] but not together.

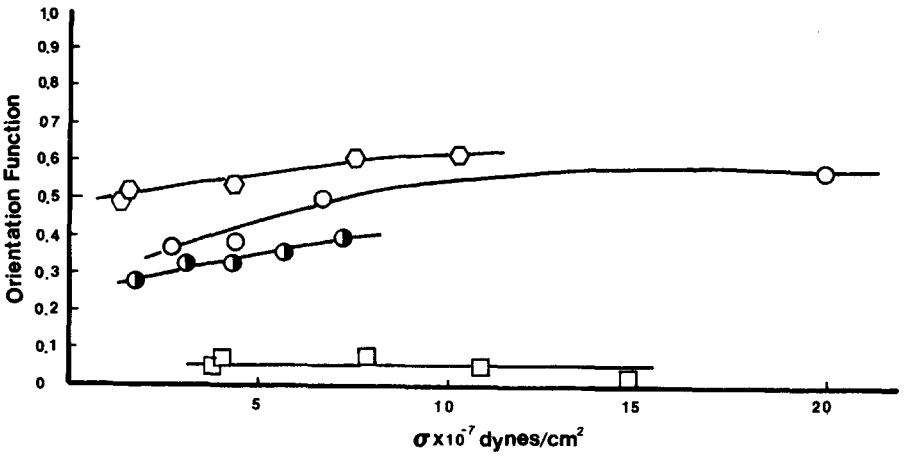

Fig. 20. Hermans orientation factors for nylon 6 components of PP/N6 blends as a function of spinline stress: (○) N6; (○) PP/N6 25/75; (◑) PP/N6 50/50; (□) PP/N6 75/25.

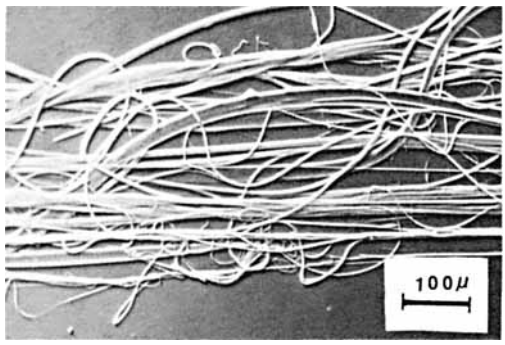

(a)

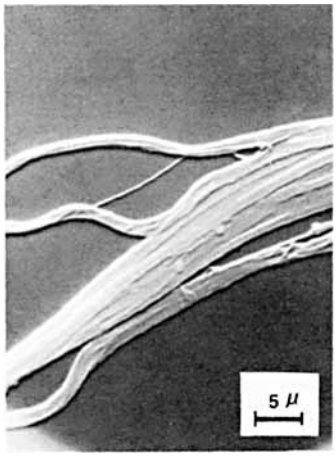

(b)

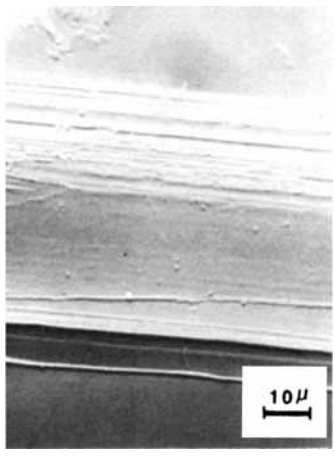

(c)

Fig. 21. Formic acid-extracted PP/N6 blend melt-spun fibers. Drawdown $v_L/v_0 = 216$: (a) 25/75; (b) 50/50; (c) 75/25.

The diameter of the minifibers can be computed from the diameters of the "islands" in the extrudates by continuity. Taking subscript o to represent the die and L the drawdown of the fiber at the takeup, we may write (neglecting density variations)

$$\tfrac{1}{4}\pi d_o^2 v_o = \tfrac{1}{4}\pi d_L v_L \tag{12}$$

This is equivalent to

$$d_L = \frac{1}{\sqrt{v_L/v_o}}\, d_o \tag{13}$$

Thus a drawdown ratio of 100 will reduce the diameters of the islands an order of magnitude in forming minifilaments. Our 25/75 system had island diameters of order 20 μm at the extrusion rate in question and a v_L/v_o of 216. The minifilament diameter of 0.5–5.0 μm is consistent with eq. (13).

This research was supported in part by the National Science Foundation, Division of Materials, Polymers Program.

References

1. P. V. Papero, E. Kubu, and L. Roloan, *Textile Res. J.*, **37,** 823 (1967).
2. B. T. Hayes, *Chem. Eng. Prog.*, **65** (10) 50 (1969).
3. J. Sibilia, *J. Appl. Polym. Sci.*, **17,** 2911 (1973).
4. K. Hayashida, J. Takahashi, and M. Matsui, *Proc. 5th Int. Rheol. Cong.*, **4,** 525 (1969).
5. F. Ide and A. Hasegawa, *J. Appl. Polym. Sci.*, **18,** 963 (1974).
6. N. K. Baramboim and V. F. Rakityanskii, *Kolloidn. Zh.*, **36,** 129 (1974).
7. M. V. Tsebrenko, M. Jakob, M. Yu. Kuchinka, A. V. Yudin, and G. V. Vinogradov, *Int. J. Polym. Mater.*, **3,** 99 (1974).
8. T. I. Ablazova, M. V. Tsebrenko, A. V. Yudin, G. V. Vinogradov, and B. V. Yarlykov, *J. Appl. Polym. Sci.*, **19,** 1781 (1975).
9. G. V. Vinogradov, B. V. Yarlykov, M. V. Tsebrenko, A. V. Yudin, and T. I. Ablazova, *Polymer*, **16,** 609 (1975).
10. M. V. Tsebrenko, A. V. Yudin, T. I. Ablazova, and G. V. Vinogradov, *Polymer*, **17,** 831 (1976).
11. A. Y. Coran and R. Patel, *Rubber Chem. Technol.*, **53,** 781 (1980).
12. T. Kitao, H. Kobayoshi, S. Ikegami, and S. Ohya, *J. Polym. Sci., Polym. Chem. Ed.*, **11,** 2633 (1973).
13. K. Walters, *Rheometry*, Chapman and Hall, London, 1977.
14. J. L. White, in *Rheometry: Industrial Applications*, K. Walters, Ed., Wiley, New York, 1980.
15. E. B. Bagley, *J. Appl. Phys.*, **24,** 627 (1957).
16. W. Minoshima, J. L. White, and J. E. Spruiell, *J. Appl. Polym. Sci.*, **25,** 287 (1980).
17. G. Natta and P. Corradini, *Nuovo Cimento Suppl.*, **15,** 40 (1960).
18. A. Ziabicki, *Kolloid Z.*, **167,** 132 (1960).
19. D. C. Vogelsong, *J. Polym. Sci. A*, **1,** 1955 (1963).
20. J. P. Parker and P. H. Lindenmeyer, *J. Appl. Polym. Sci.*, **21,** 821 (1977).
21. R. S. Stein, *J. Polym. Sci.*, **31,** 327 (1958).
22. H. P. Nadella, H. M. Henson, J. E. Spruiell, and J. L. White, *J. Appl. Polym. Sci.*, **21,** 3003 (1977).
23. V. G. Bankar, J. E. Spruiell, and J. L. White, *J. Appl. Polym. Sci.*, **21,** 2341 (1977).
24. Z. W. Wilchinsky, *J. Appl. Phys.*, **30,** 792 (1959); **31,** 1969 (1960); *Adv. X-Ray Anal.*, **6,** 231 (1963).
25. K. Oda, J. L. White, and E. S. Clark, *Polym. Eng. Sci.*, **10,** 25 (1978).
26. W. Minoshima, J. L. White, and J. E. Spruiell, *Polym. Eng. Sci.*, **20,** 1166 (1980).
27. H. Yamane and J. L. White, *Polym. Eng. Rev.*, **2,** 167 (1983).
28. K. Min, J. L. White, and J. F. Fellers, unpublished research.
29. G. I. Taylor, *Proc. Roy. Soc. A*, **146,** 501 (1934).
30. S. Tomotika, *Proc. Roy. Soc. A*, **150,** 322 (1935); **153,** 302 (1936).
31. F. D. Rumscheidt and S. G. Mason, *J. Colloid Sci.*, **16,** 238 (1961).
32. C. Lees, *Proc. Phys. Soc.*, **17,** 460 (1900).
33. J. E. Spruiell and J. L. White, *Polym. Eng. Sci.*, **15,** 660 (1975).
34. C. H. Chen, J. L. White, J. E. Spruiell, and B. C. Goswami, *Text. Res. J.*, **53,** 44 (1983).
35. J. Gianchandani, J. E. Spruiell, and E. S. Clark, *J. Appl. Polym. Sci.*, **27,** 3527 (1982).
36. K. Katayama, T. Amano, and K. Nakamura, *Kolloid Z. Z. Polym.*, **226,** 126 (1967).
37. W. A. Miller and C. N. Merriam, U. S. Pat. 3,097,991 (1963).
38. C. N. Merriam and W. A. Miller, U. S. Pat. 3,099,067 (1963).
39. H. D. Anspon, B. H. Clampitt, D. G. Ashburn, and F. E. Brown, Br. Pat. 1,200,676 (1969).
40. M. V. Tsebrenko, M. Jakob, M. Yu. Kuchinka, and A. V. Yudin, *Int. J. Polym. Mater.*, **3,** 99 (1974).
41. J. Shimizu, N. Okui, T. Yamamoto, M. Ishi, and A. Takatu, *Sen-i-Gakkaishi*, **38,** T-1 (1982).

Received December 29, 1982
Accepted January 14, 1983